REVISED Manuscript (text UNmarked in Editable Format)

Click here to view linked References

Tribological Property of ta-CNx:Ta Deposited via Ion Beam Assisted-Filtered Arc Deposition

T. Tokoroyama [1*], Y. Tagami[1], M. Murashima[1], W.-Y. Lee[1], N. Umehara[1], H. Kousaka[2]

[1)] Department of Micro-Nano Mechanical Science and Engineering,
Graduate School of Engineering, Nagoya University,
Furo-cho, Chikusa-ku, Nagoya, Aichi 464-8603, Japan
[2)] Graduate School of Natural Science and technology, Gifu University,
1-1, Yanagito, Gifu-shi, Gifu 501-1193, Japan

[*]Corresponding authors: takayuki.tokoroyama@mae.nagoya-u.ac.jp
Telephone: +81 52 789 2787

Abstract

Improving the hardness of amorphous carbon nitride with tantalum was realized by using ion beam assisted filtered arc deposition to obtain a low friction coefficient and low specific wear rate in ambient air. The coatings were prepared with different nitrogen flow during coating at different discharge cycles of tantalum. The wear scar and as-deposited surfaces were observed and analyzed by means of FESEM, AES, XPS, and Raman analysis. The lowest friction coefficient (~0.07) was obtained for ta-C:Ta200, which exhibited a low specific wear rate of $<1.0\times10^{-7}$ mm^3/Nm. The XPS analysis revealed the existence of amorphous Ta_2O_5, and the friction coefficient seemed to be positively correlated with oxygen desorption from the coatings.

Keywords: tantalum doped DLC; CNx; low friction; anti-oxidation

1. Introduction

Carbonaceous hard thin coatings referred to as DLC (diamond-like carbon) have attracted attention as materials capable of exhibiting a low friction coefficient and high wear resistance in various atmospheres. Several types of carbonaceous coatings exist, the friction coefficient and wear property are strongly depending on which type of coating do you use and what the friction test surroundings is. In the case of using DLC coating in lubricants, we should consider that several pairs of a coating and an additive have undesirable wear acceleration and high friction coefficient. Haci et al. reported that tetrahedral amorphous carbon (ta-C) with glycerol mono-oleate (GMO) and zinc dialkylditiophosphate (ZnDTP) did not show low friction under boundary lubrication [1]. Kassim et al. reported that molybdenum materials derived from molybdenum dithiocarbamate (MoDTC) can accelerate wear of hydrogenated DLC (a-C:H), especially for Mo_2C as an abrasive, MoO_3 as a coatings' oxidation [2, 3]. Especially for non-hydrogenated carbonaceous coatings, main mechanism of low friction was assumed the existence of graphite domain at the topmost surface. Heimberg et al. reported the friction force between graphite plane surface and tungsten carbide (WC) tip which was strongly depended on sliding direction. The friction force became large when the tip slid a commensurate phase direction, and it became small when it slid an incommensurate phase [4]. Such graphite structure (or graphite domain) on the topmost surface of carbonaceous coating is important key to generate low friction coefficient. Therefore, several observation techniques were pursued to reveal existence of sp^2/sp^3 orbitals of coatings during friction by in-situ reflect spectroscopy [5, 6], surface enhanced Raman spectrometry (SERS) to obtain only surface information from the topmost surface (less than approximately 1.7 nm depth) [7], in-situ Raman analysis to understand additives' structural change and relation between those additives and DLC coating [8], and so on. Graphitization is one of the keys to generate low friction with high hardness substrate.

The wear mechanism of DLC is divided roughly two as mechanical and chemical wear. Cyclic impact induced sp^2 cluster size reduction of a-C coating which is associated to mechanical wear [9, 10], carbon atoms diffusion to a mating material was reported [11–13], and it was strongly depended on counterpart material affinity/solubility to carbon which is associated to chemical wear. To prevent such mechanical and chemical wear, we synthesized ta-C to reduce its defects [14–16], to reduce large delamination by structured ta-C [17, 18], to improve mechanical and chemical properties by doping several atoms such as nitrogen [19, 20], silicon, chromium, boron [21, 22], and tantalum [23, 24]. Especially for the Ta included a-C coating showed low friction coefficient under ambient air [24], however, the coating hardness was insufficient (around 10 GPa), so obtaining Ta included high hardness type coating is demanded to use in ambient air. Our first target of this research is applying Ta doping to ta-C by IBA-FAD (ion beam assisted-filtered arc deposition) combined with another FAD source was used to synthesize tetrahedral-type CNx with Ta (so-called ta-CNx:Ta), to obtain hardness higher than 10 GPa which value is reported by authors as Ta and nitrogen included in a-C.

The second target of this research is to investigate low friction coefficient ability of Ta, nitrogen included ta-C coatings (so-called ta-C:Ta, ta-CNx:Ta). The authors reported that the inclusion of Ta or other elements in the carbon structure resulted in a low friction coefficient in ambient air [23, 24], although DLC and/or CNx generally did not perform low friction coefficient less than around 0.1 under ambient air [25–27]. The cause of "not low friction" was assumed that oxygen could adhere graphite edge or dangling bond to enhance its wear and rise friction [26, 28–30]. Especially the literature reported by Kelemen et al. [30] that O_2 adsorbs damaged graphite or edge easier than plane of graphite. It implies that low friction phenomena of DLC or CNx because of graphite like structure can be prolonged if DLC or CNx has some element which can prevent O_2 adsorption to graphite edges or dangling bonds in a coating. The tribological properties of the material were investigated via friction tests. After these tests, the surfaces were observed and analyzed by means of FESEM (field emission scanning electron microscopy), AES (Auger electron spectroscopy), and Raman spectroscopy. Finally, low friction maintaining mechanism was discussed.

2. Experimental procedure

2.1 ta-CNx:Ta coating process and materials properties

The samples of ta-CNx:Ta were prepared using laboratory equipment, such as an IBA-FAD system, the schematic is shown in Fig. 1 [31]. To ionize the carbon, arc discharge is applied to the carbon target used as the cathode. The ionized carbon contains neutral particles, which were removed by deflecting the beam direction by 90° using a magnetic field, and only the ionized carbon was irradiated to the samples. A ta-CNx:Ta coating was synthesized by means of a dynamic mixing method. This method mixes carbon, nitrogen, and tantalum by irradiating a nitrogen ion beam from a microwave ion source and then irradiating a tantalum ion beam from an arc plasma source. The coating vacuum chamber was evacuated by rotary and turbo molecule pump to reach 5.0×10^{-4} Pa as back pressure. The carbon target was pre-arced before coating procedure to clean target surface by 50 A pre-arc ampere and 15 V duct bias voltage. Consequently, the substrate was cleaned by Ar ion-beam bombardment by 20 sccm Ar gas flow and substrate bias voltage of −100 V at first, then the voltage increased to −600 V during 2 min. The bombardment process was conducted twice to clean the substrate surface to prevent peel-off. After the cleaning procedure, 20 min. interval was applied to cool the substrate in high vacuum. The ta-C:Ta coating was conducted by the parameters listed in Table 1. The coating procedure was 20 cycles of 1 min. deposition and 2 min. interval because of temperature rise suppression of the substrate, and a ta-CNx:Ta coating thickness of ~200 nm was realized. The carbon target and Ta target are provided from Kojundo Chemical Lab. Co., Ltd. Japan. Each target purity is higher than 99.9%. The sample preparation with using nitrogen ion beam and Ta ion beam source were independently controlled. The Ta doping to a ta-CNx:Ta coating was conducted by an arc plasma gun (Ulvac, ARL-300, Japan). To

achieve the desired Ta concentration, an arc deposition frequency ranging from 0 to 200 pulse/min was employed. Nitrogen ion beam was generated by another ion beam source (Alios, EMIS-221, Japan) with using a microwave power source (Alios, MP-201B, Japan). A 2.45 GHz microwave and magnets can generate electron cyclotron resonance at a plasma chamber, then it was extracted by several acceleration cathodes. The nitrogen ion beam was controlled by flow rate of nitrogen gas as 0, 3, and 5 sccm (standard cubic centimeter). The friction pair of substrates included a SUJ2 (stainless steel) ball (diameter: 8.0 mm) and a SUJ2 disk (diameter: 22.5 mm and thickness: 4 mm). The resulting samples were referred to as ta-CN5:Ta200 corresponding to a N_2 gas supply of 5 sccm and a Ta arc deposition frequency of 200 pulse/min. The sample names and the atomic percentage of C, N, O and Ta are listed in Table 2 (detailed explanation presented in section 3.1). The atomic percentage of each coating was measured via x-ray photoelectron spectroscopy, (XPS; Ulvac phi Quantera II) with an Al Kα monochromatic x-ray source under vacuum lower than 10^{-5} Pa. Prior to measurements of the topmost surface, Ar ion beam sputter cleaning was performed (acceleration voltage: 4 kV) on an ~2 mm^2 area. Afterward, XPS measurements were performed (acceleration voltage: 15 kV and power: 25 W) on an ~100 μm^2 area. Wide peak measurements for 1 to 1100 eV with 1.0 eV/step were conducted to confirm all elements. In addition, narrow peak measurements for energy ranging from 280.0 to 295.0 eV, 392.0 to 410.0 eV, and 18.0 to 38.0 eV for C1s, N1s, and Ta_4f, respectively, were conducted at 0.1 eV/step. The hardness of each coating was measured using a nanoindentation tester (ENT-1100a, Elionix). The Berkovich type diamond tip applied a force of 1000 μN to each coating surface for 1 s holding time at the highest normal load. The summary of main coating and experimental procedures are summarized in Fig. 2.

-Figure 1-

-Table 1-

-Table 2-

-Figure 2-

2.2 Friction test procedure by using ball-on-disk friction tester and analysis equipment conditions

The friction test used in this study is ball-on-disk type [31]. The normal load was applied by a dead weight of 1.0 N. The ball specimen was fixed by a ball holder during the tests, and the friction force was measured by a load cell. A flow of dry air (~5 L/min) to the contact between the ball and the disk specimen occurred during each friction test without any additional force detected by the load cell. The load cell can obtain frictional force by applying the force at the contact point through the bar with the pivot. The gap between the gas flow port and specimen was ~5 mm with the flow direction perpendicular to the sliding direction. The employed sliding speed (150 rpm) and rotation radius (4 mm) corresponded to a sliding speed of ~62.8 mm/s. All friction tests were conducted for 5 min at room

temperature (23–24°C). The friction test pairs were same coating synthesized on a SUJ2 ball and a SUJ2 disk (such as ta-CN5:Ta200 coated ball vs. ta-CN5:Ta200 disk). After the friction tests, the wear scar diameter was determined via optical microscopy. The wear volume was then calculated from the wear scar diameter by considering geometric factors (e.g., as the wear loss volume was assumed to be portion of spherical).

Moreover, AES (PHI-650, Perkin-Elmer) measurements were conducted under high vacuum pressure (lower than 1.0×10^{-7} Pa). An acceleration voltage and current of 5.0 kV and 100 nA, respectively, were employed. In addition, 20 cycle measurements from 150 to 550 eV with 0.2 eV/step were conducted and accumulated. The highest intensity was C KLL as peak position is 275.0 eV, O KLL as 389.0 eV, and N as 510.0 eV. The gap between the highest peak intensity of C KLL and the lowest of C KLL was determined to a normalization, and then we calculated the atomic percentage ratio of N/C and O/C.

The I_D and I_G peaks were measured via Raman analysis (NRS-1000, Jasco) performed at a wavelength of 530.3 nm and power of 10 mW for wavenumbers ranging from 800 to 2000 cm^{-1}. Each measurement was conducted twice to eliminate undesirable noise from outer space.

3. Results

3.1 XPS analysis for ta-CNx:Ta

The effect of Ta arc discharges on the covalent bonds between Ta and other elements was analysed. The results presented in Fig. 3(a) to (c) show different pulses with different N_2 flow during the synthesis process. The peak of ~25 eV corresponds to $Ta_4f_{5/2}$ and $Ta_4f_{7/2}$. Other peaks occurring at 226, 238, and 401 eV are also Ta peaks, indicating that the discharge method can introduce Ta into the ta-CNx coating. The narrow peak of C1s and others corresponded to ta-C with sp^2 (C1: 284.4 eV), sp^3 or aliphatic (C2: 285.0 eV), and hydroxyl (C3: 286.3 eV). For the Ta-containing materials, the peaks corresponded to Ta–C: 283.6-284.1 eV, sp^2 and sp^3 C–C type bonds (C1: 284.4 eV), sp^2 C=N (C2: 286.2 eV), and the sp^3 bond of C–N (C3: 287.8 eV) [24], [32, 33].

-Figure 3-

The representative C1s peaks are shown in Fig. 4(a) as ta-C (without N_2 flow and Ta discharge), (b) as ta-C:Ta200, (c) as ta-CN5, and (d) as ta-CN5:Ta200. The Ta and C detailed bonding is shown in Fig. 5(a) to (e) corresponding to the results shown in Fig. 4. The results of the material without the Ta discharge (i.e., ta-C) are shown in Fig. 5(a). No clear Ta peak was observed. The effect of the Ta discharge and the N_2 flow effect on the coatings is shown as Fig. 5(b) ta-C:Ta200, (c) ta-CN5, (d) ta-CN5:Ta100, and (e) ta-CN5:Ta200.

The Ta discharges revealed the occurrence of Ta in the coatings, but the N_2 flow had little effect

on the Ta_4f peak (compare (b) and (e)). Additionally, the discharge effect on the Ta peak intensities is manifested as a significant increase in the intensity of Ta (Fig. 5(c) to (e). The gap between the main two peaks is 1.8 eV ($Ta_4f_{5/2}$: 25.2 eV, $Ta_4f_{7/2}$: 23.3 eV) [24, 34].

The N1s peaks are shown in Fig. 6(a) to (d). The peaks of pyridine-like C–N=C bonds (398.5–398.6 eV) [35] and TaNx (402–403 eV) [36] were considered. The ta-C (Figure 6(a)) and ta-C:Ta200 (Fig. 6(b)) peaks were compared, and clear sp^2 C=N (400 eV) was observed only for the Ta discharge coating. Furthermore, the N_2 flow effect of N1s on ta-CN5 is shown in Fig. 6(c). The peak intensity was slightly larger than that of the only ta-C material (see Fig. 6(a)), and the peak was attributed to the splitting of two peaks such as those corresponding to pyridine-like C–N=C and sp^2 C=N. The ta-CN5:Ta200 material was strongly affected by the Ta discharge and N_2 flow as shown in Fig. 6(d), where clear TaNx, pyridine-like C–N=C, and TaOxNy (402.6 eV) [36] peaks are observed.

-Figure 4-

-Figure 5-

-Figure 6-

3.2 Hardness of coatings and Raman analysis results before friction

The hardness and Young's modulus are listed in Table 3. The hardness decreased slightly (from 42 to 39 GPa) with increasing N_2, whereas the Young's modulus decreased significantly (from ~415 to 290 GPa). Ta inclusion in the coating led to reductions in the hardness and Young's modulus, owing possibly to reductions in the sp^3 content accompanying the formation of other covalent bond types in the coating (see above section).

The Raman analysis results of representative coatings are shown in Fig. 7(a) to (d); these correspond to the coating results shown in Fig. 4. Each peak was deconvoluted to an I_D peak and an I_G peak at ~1330 cm^{-1} and ~1580 cm^{-1}, respectively. A comparison of the ta-C (Fig. 7(a)) and ta-C:Ta200 (Fig. 7(b)) peaks indicated that including Ta in the coatings led to deterioration of the Raman signal. The assumption is that the inclusion of Ta affected the carbon structure through (for example) reduction in the size of the carbon-carbon covalent bond network. However, including N in the coating had only a modest effect on the Raman data (see ta-CN5 in Fig. 7(c)). The inclusion of Ta in the coating had considerable effect on the data. This effect was manifested as a high I_D peak intensity and signal noise, as shown in Fig. 7(b) for the Ta-including material. The high intensity may have resulted from hardness reduction associated with increasing sp^2 C=C hybridization or small fragmentation of the carbon-carbon network [37].

-Table 3-

-Figure 7-

3.3 Tribological properties of coated ball and coated disks

Friction tests on coated balls and coated disks were conducted at room temperature under an atmosphere of dry air. Representative friction coefficient values of the balls and disks are shown in Fig. 8(a) as ta-C, (b) ta-C:Ta200, (c) ta-CN5, and (d) ta-CN5:Ta200. After each friction test, the ball surfaces were observed via FESEM (see corresponding images in Fig. 9(a) to (d)). Determining the specific wear rate of the disks was difficult, owing to the low wear experienced by each disk. The specific wear rate of the ball specimens was calculated from the observed wear scar diameter. The wear rates as a function of the inverse coating hardness is shown in Fig. 10(a), and the average friction coefficient from 150 to 750 cycles is shown in Fig. 10(b). Almost all the rates were $<1.0\times10^{-7}$ mm^3/Nm, which lies in the mild wear regime. In addition, the specific wear rate of ta-C with Ta (shown by circle) decreased with decreasing hardness. Generally, the specific wear rate is inversely proportional to the hardness. The results suggested that both the ta-C coated ball and disk specimens were excessively hard, and hence, maintaining each coating during the friction test was difficult. This was especially true for the balls, which experienced more severe friction than the disks, owing to continuous contact with the mating surface. The effect of N in the coatings on the specific wear rate was unclear (shown as circle, triangle, and square; a sharp trend with increasing N was absent). The hardness of the Ta-containing materials decreased with increasing amount of Ta (shown as black and white, gray, and black). Furthermore, the average friction coefficient was only slightly proportional to the coating hardness. From the viewpoint of ta-C with Ta, the hardness reduction occurred primarily at low friction levels. The hardness of the ta-CNx:Tay coating was higher than that of the coating without N, and the average friction coefficient was slightly higher.

The average friction coefficient and specific wear rate results of the coated balls are summarized in Fig. 11. The friction coefficient decreased with increasing amount of Ta in the Ta-containing ta-C coatings (shown as circles), but increased (in general) in the case of the N-containing coatings. The lowest friction coefficient (~0.07) was obtained for the ta-C:Ta200.

-Figure 8-

-Figure 9-

-Figure 10-

-Figure 11-

3.4 Raman analysis of coated balls after friction tests

After the friction tests, Raman analysis was performed on the coated disks and balls (see Fig. 12(a) to (d) for representative examples). The disks before and after testing were almost identical, and hence, are excluded from further discussion. In contrast, the coated balls exhibited significant

differences after testing. In the case of ta-C, the I_D peak increased sharply as shown in Fig. 12(a). The effect of Ta was evident in Fig. 12(b), even without a considerable I_D peak increment. An I_D peak increment was, however, observed for ta-CN5 (see Fig. 12(c)). No clear increment was observed for the Ta- and N-containing ta-CN5:Ta200 material. The lack of I_D peak increment in the coatings without Ta may have resulted from the lower level of graphitization occurring in these materials compared with that occurring in the ta-C or ta-CN series.

-Figure 12-

3.5 AES analysis of the coated balls before and after friction tests

The coated balls before and after the friction tests were compared through AES analysis (see Fig. 13(a) to (d) for representative examples). Testing led to only slight differences in ta-C (Fig. 13(a)). In the case of ta-C:Ta200 (Fig. 13(b)), the O KLL peak intensity decreased with testing. Moreover, a considerable N KLL peak loss was observed for ta-CN5, indicating nitrogen atom desorption from the material, as previously reported [38]. N KLL peak and O KLL peak losses were observed for ta-CN5:Ta200 (Fig. 13(d)) suggesting that nitrogen atom desorption, and some oxidative molecule desorption (involving Ta oxide) occurred in this material.

-Figure 13-

4. DISCUSSION

From the viewpoint of N KLL and O KLL peak intensity change during the friction tests, we summarized the N/C and O/C ratios of each coating from AES data (see Fig. 14(a) and (b)). The series of ta-C to ta-C:Ta200 contained no N and the N/C ratios before and after the tests were lower than 0.02. This value indicated that the topmost surface of the coating contained almost no nitrogen (generally the depth was <5 nm) [39]. The N content of ta-CN3 with Ta series and ta-CN5 with Ta series decreased after the friction tests. This result is consistent with the previously reported [38] “desorption of nitrogen” phenomenon. Such light element in carbonaceous coating was reported several authors [40–42]. Previously, we revealed that nitrogen atoms incorporated in the CNx desorbed when it slid against a Si_3N_4 ball in N_2 environment. The nitrogen desorption was assumed to be happened by breaking C–N covalent bonds by flash temperature or tribochemical reaction generated from tribomicroplasma [43]. Tribomicroplasma generally includes visible, infrared (IR), and ultraviolet (UV) light. Therefore, IR and UV have possibility to break several covalent bonds in those coatings. After or during friction tests, there was no clear temperature increase, so UV is assumed one of the triggers to break covalent bonds. Our previous experiments proved tribomicroplasma generation under N_2 from CNx coating [44], and 254, 312, and 365 nm UV irradiation affect the CNx that nitrogen desorption by UV irradiation and transmission electron microscope with electron diffraction pattern revealed the

formation of graphite domains [45].

From the viewpoint of O in the coatings, a friction-induced increase in O occurred only in ta-CN3 and ta-CN5 (see Fig. 14(b)). The differences between the N/C and O/C ratios before and after the friction tests (ΔN/C and ΔO/C) were calculated. Afterward, the effect of these differences on the specific wear rate and the average friction coefficient was investigated (see Fig. 15(a) to (b) and Fig. 16(a) to (b)). ΔN/C and ΔO/C had almost no effect on the specific wear rate, and ΔN/C had only a small effect on the average friction coefficient, as evidenced by an R2 value of <0.28. However, ΔO/C ratio had a considerable effect on the friction coefficient (R2 = 0.55). This result indicated that oxygen desorption from the coating affected the low friction orientation at the topmost surface, as reported in a previous study [19]. The XPS spectra of each Ta-containing coating consisted of two clear peaks (see Fig. 5(b), (d), and (e)). Peaks corresponding to $Ta_4f_{7/2}$ and $Ta_4f_{5/2}$ from Ta_2O_5 [46] were observed, and the O1s peak revealed that the Ta-only coatings gave rise to an O KLL peak at ~530 eV, which corresponds to pure Ta_2O_5 [47]. Raman analysis of the coating including Ta indicated that the Raman shift data was noisier than that of the coating without Ta. This implied that the carbon network was affected by Ta, Ta-carbide or Ta_2O_5 incorporated into the coatings. From the viewpoint of Raman analysis data (Fig. 12) and friction coefficient with ΔO/C in Fig. 16, ta-C and ta-CN5 showed higher friction coefficient rather than ta-C:Ta200. Both ta-C and ta-CN5 showed clear two peaks related to I_D and I_G, it indicated carbon network disordering [48–50]. On the other hand, ta-C:Ta200 did not show such peak separation, therefore, the most part of carbon structure in ta-C:Ta200 did not change.

In the case of Ta_2O_5 is adjacent to carbon atoms, oxygen desorption is likely to be happened and a vacancy is generated [51]. Above mentioned Ta_2O_5 in the coating naturally grew after deposition process. Therefore, if the oxygen desorption by friction was taken place, it has a possibility of oxidization again. Such Ta-oxidation and oxygen desorption repeatability are assumed to protect graphite edges or dangling bonds because of less possibility of carbon oxidation. Regarding the role of nitrogen, the I_D peak intensity increased when a N_2 flow was applied during the coating synthesis procedure. The hardness reduction was attributed mainly to nitrogen incorporation between the carbon-carbon network and carbon-X (X = Ta, O, N) network. No X-ray diffraction studies were performed in this work. However, the assumption was that the Ta-containing species were the amorphous phase based on the high carbon content and low N_2 flow, as reported in previous studies [52, 53].

-Figure 14-

-Figure 15-

-Figure 16-

5. CONCLUSIONS

Previously, Ta incorporated a-C type coating showed low friction coefficient in ambient air, however, the low friction phenomena did not maintain due to low hardness of the coating. Therefore, we changed most part of carbon structure in the coating to tetrahedral type to reach hardness higher than 10 GPa. The separated coating sources such as ionized carbon, nitrogen ion beam, and sputtered Ta were mixed on SUJ2 balls and SUJ2 disks. Friction tests under ambient air between same coating pairs were conducted, then XPS, AES, Raman analysis as well as nano-indentation hardness measurements were conducted. Obtained main results are shown below.

Ta included ta-C and ta-CNx were successfully synthesized on SUJ2 balls and SUJ2 disks. The highest hardness of the coating (i.e. ~42.4 GPa) was obtained without any nitrogen and Ta. Incorporation of both Ta and N led to hardness reduction of the coatings. However, the lowest hardness of ta-CN5:Ta200 showed approximately 18 GPa. Therefore, obtaining hard coatings higher than 10 GPa by IBA-FAD was realized.

The tribological properties of the coating pair under ambient air were investigated. Almost all coating pairs exhibited a small specific wear rate ($<1.0\times10^{-7}$ mm^3/Nm) of the coated ball. The lowest friction coefficient (~0.07) was obtained for the ta-C:Ta200 coating.

The low friction mechanism was investigated by XPS, AES, and Raman analysis. The XPS analysis revealed each Ta incorporated coatings have Ta–C covalent bond. AES analysis performed before and after the friction tests indicated that oxygen desorption from the wear scar was occurred. The oxygen desorption ratio based on carbon (ΔO/C) had a considerable effect on the friction coefficient. From the viewpoint of Raman analysis, ta-C and ta-CN5 showed higher friction coefficient rather than ta-C:Ta200. Both ta-C and ta-CN5 showed clear two peaks related to I_D and I_G, it indicated carbon network disordering.

References

[1] Tasdemir HA, Wakayama M, Tokoroyama T, Kousaka H, Umehara N, Mabuchi Y, Higuchi T. Ultra-low friction of tetrahedral amorphous diamond-like carbon (ta-C DLC) under boundary lubrication in poly alpha-olefin (PAO) with additives. Tribol Int 2013;65:286–94. https://doi.org/10.1016/j.triboint.2013.03.014.

[2] Kassim KAM, Tokoroyama T, Murashima M, Umehara N. The Wear Classification of Molybdenum-derived Particles on Silicon and Hydrogenated Diamond-Like Carbon at Room Temperature. Tribol Int 2020;147:106176. https://doi.org/10.1016/j.triboint.2020.106176.

[3] Kassim KAM, Tokoroyama T, Murashima M, Lee W.-Y, Umehara N, Mustafa MMB. Wear acceleration of a-C:H coatings by Molybdenum-derived particles: Mixing and temperature effects. Tribol Int 2021;159:106944. https://doi.org/10.1016/j.triboint.2021.106944.

[4] Dienwiebel M, Verhoeven GS, Pradeep N, Frenken JWM, Heimberg JA, Zandbergen HW.

Superlubricity of Graphite. Phys. Rev. Lett. 2004;92:126101. https://doi.org/10.1103/PhysRevLett.92.126101.

[5] Ohara K, Masuripan NAB, Umehara N, Kousaka H, Tokoroyama T, Inami S, Zushi K, Fujita M. Evaluation of transformed layers of DLC after sliding in oil with spectroscopic reflectometry. Tribol Int. 2013;65:270–7. https://doi.org/10.1016/j.triboint.2013.01.010.

[6] Nishimura H, Umehara N, Kousaka H, Tokoroyama T. Clarification of relationship between friction coefficient and transformed layer of CNx coating by in-situ spectroscopic analysis. Tribol Int 2016;93:B:660–5. https://doi.org/10.1016/j.triboint.2014.12.015.

[7] Tokoroyama T, Murashima M, Umehara N. The Surface Enhanced Raman Scattering analysis for carbonaceous coating by using Au Nano-Particles. Tribology Online;202015:300–8. https://doi.org/10.1016/j.triboint.2014.12.015.

[8] Ohkubo H, Sasaki S. In situ Raman observation of structural transformation of diamond-like carbon films lubricated with MoDTC solution: Mechanism of wear acceleration of DLC films lubricated with MoDTC solution. Tribol Int 2017;113:399–410. https://doi.org/10.1016/j.triboint.2016.10.009.

[9] Abdollah MFB, Yamaguchi Y, Akao T, Inayoshi N, Umehara N, Tokoroyama T. Phase Transformation Studies on a-C Coating under Repetitive Impacts. Surf Coat Technol 2010;205:2:625–31. https://doi.org/10.1016/j.surfcoat.2010.07.062.

[10] Abdollah MFB, Yamaguchi Y, Akao T, Inayoshi N, Miyamoto N, Tokoroyama T, Umehara N. Deformation-wear transition map of DLC coating under cyclic impact loading. Wear 2012;274–275:27:435–41. https://doi.org/10.1016/j.wear.2011.11.007.

[11] Aboua KAM, Umehara N, Kousaka H, Tokoroyama T, Murashima M, Mabuchi Y, Higuchi T, Kawaguchi M. Effect of carbon diffusion on friction and wear behaviors of diamond-like carbon coating against Cr-plating in boundary base oil lubrication. Tribology Online 2018;13:290–300. https://doi.org/10.2474/trol.13.290.

[12] Aboua KAM, Umehara N, Kousaka H, Tokoroyama T, Murashima M, Mustafa MMB, Mabuchi, Y, Higuchi T, Kawaguchi M. Effect of mating material and graphitization on wear of a-C:H coating in boundary base oil lubrication. Tribology Letters 2020;68:24. https://doi.org/10.1007/s11249–019–1248–6.

[13] Aboua KAM, Umehara N, Kousaka H, Tokoroyama T, Murashima M, Mabuchi M, Higuchi T, Kawaguchi M. Effect of Carbon Diffusion on Friction and Wear Behaviors of Diamond-Like Carbon Coating Against Germanium in Boundary Base Oil Lubrication. Triblogy Letters 2019; 67:65. https://doi.org/10.1007/ s11249–019–1179–2.

[14] Lee WY, Tokoroyama T, Jang YJ, Umehara N. Effect of substrate bias and temperature on friction and wear properties for ta-C coating prepared under different substrate bias voltages with filtered cathodic vacuum arc deposition. Tribology Online 2018;13:5:241–7.

https://doi.org/10.2474/trol.13.241.

[15] Lee WY, Tokoroyama T, Jang YJ, Umehara N. Investigating running-in behavior to understand wear behavior of ta-C coating with filtered cathodic vacuum arc deposition. Journal of Tribologi 2019;23:38–47.

[16] Lee WY, Jang YJ, Umehara N, Tokoroyama T, Murashima M. Effect of defects on wear behavior in ta-C coating prepared by filtered cathodic vacuum arc deposition. Diam Relat Mater 2020;105:107789. https://doi.org/10.1016/j.diamond.2020.107789.

[17] Mustafa MMB, Umehara N, Tokoroyama T, Murashima M, Shibata A, Utsumi Y, Moriguchi H. Effect of pillar and mesh structure of tetrahedral amorphous carbon ta-C coatings on the wear properties and fracture toughness of the coating. Tribology Online 2019;14:5:388–97. https://doi.org/10.2474/trol.14.388.

[18] Mustafa MMB, Umehara N, Tokoroyama T, Murashima M, Shibata A, Utsumi Y, Moriguchi H. Effect of mesh structure of tetrahedral amorphous carbon ta-C coating on friction and wear properties under base-oil lubrication condition. Tribol Int 2020;147:105557. https://doi.org/10.1016/j.triboint.2019.01.016.

[19] Liu X, Yamaguchi R, Umehara N, Murashima M, Tokoroyama T. Effect of oil temperature and counterpart material on the wear mechanism of ta-CNx coating under base oil lubrication. Wear 2017;390–391:312–21. https://doi.org/10.1016/j.wear.2017.08.012.

[20] Liu X, Umehara N, Tokoroyama T, Murashima M. Tribological properties of ta-CNx coating sliding against steel and sapphire in unlubricated condition. Tribol Int 2019;131:102–11. https://doi.org/10.1016/j.triboint.2018.10.022.

[21] Tasdemir HA, Tokoroyama T, Kousaka H, Umehara N, Mabuchi Y. Influence of zinc dialkyldithiophosphate tribofilm formation on the tribological performance of self-mated diamond-like carbon contacts under boundary lubrication. Thin Solid Films 2014;562:389–97. https://doi.org/10.1016/j.tsf.2014.05.004.

[22] Deng X, Kousaka H, Tokoroyama T, Umehara N. Deposition and tribological behaviors of ternary BCN coatings at elevated temperatures. Surf Coat Technol 2014;259:2–6. https://doi.org/10.1016/j.surfcoat.2014.08.087.

[23] Nyberg H, Tokoroyama T, Wiklund U, Jacobson S. Design of low-friction PVD coating systems with enhanced running-in performance - carbon overcoats on TaC/aC. Surf Coat Technol 2013; 222:48–54. https://doi.org/10.1016/j.surfcoat.2013.02.003.

[24] Tokoroyama T, Hattori T, Umehara N, Kousaka H, Manabe K, Kishi M, Fuwa Y. Ultra-low friction properties of carbon nitride tantalum coatings in the atmosphere. Tribol Int 2016;103: 388–93. https://doi.org/10.1016/j.triboint.2016.07.015.

[25] Kim DS, Fischer TE, Gallois B. The effects of oxygen and humidity on friction and wear of diamond-like carbon films. Surf Coat Technol 1991;49:537–42. https://doi.org/10.1016/0257–

8972(91)90113–B.

[26] Tokoroyama T, Nakamura T, Umehara N, Tomita H, Takenoshita Y. The effect of environmental gas on friction coefficient of CNx coatings and maximum concentration of O_2 for the realization of ultra-low friction. Tribologits. 2005;50:9:683–9.

[27] Eryilmaz OL, Erdemir A. TOF-SIMS and XPS characterization of diamond-like carbon films after tests in inert and oxidizing environments. Wear 2008;265:244–54. https://doi.org/10.1016/j.wear.2007.10.012.

[28] Bhowmick S, Lou M, Khan MZU, Banerji A, Alpas AT. Role of an oxygen atmosphere in high temperature sliding behaviour of W containing diamond-like carbon (W-DLC). Surf Coat Technol 2017;332:399–407. https://doi.org/10.1016/j.surfcoat.2017.06.093.

[29] Li H, Xu T, Wang C, Chen J, Zhou H, Liu H. Friction behaviors of hydrogenated diamond-like carbon film in different environment sliding against steel ball. Appl Surf Sci 2005;249:257–65. https://doi.org/10.1016/j.apsusc.2004.12.002.

[30] Kelemen SR, Freund H. O_2 oxidation studies of the edge surface of graphite. Carbon 1985;23:6:619–25. https://doi.org/10.1016/0008–6223(85)90221–0.

[31] Hojo K, Umehara N, Tokoroyama T, Murashima M. Effect of doped tantalum in ta-CNx film or tantalum as counterpart material on the friction and wear properties of ta-CNx. Trans JSME 2020;86:888:20–00018.

[32] Mezzi A, Kaciulis S. Surface investigation of carbon films: from diamond to graphite. Surf Int Anal 2010;42:1082–4. https://doi.org/10.1016/

[33] Kaciulis S. Spectroscopy of carbon: from diamond to nitride films. Surf Int Anal 2012;sia.4892. https://doi.org/10.1002/sia.4892.

[34] Benchikh N, Garrelie F, Wolski K, Donnet C, Fillit RY, Rogemond F, Subtil JL, Rouzaud JN, Laval JY. Nano-composite tantalum-carbon-based films deposited by femtosecond pulsed laser ablation. Thin Solid Films 2006;494:1:98–104. https://doi.org/10.1016/j.tsf.2005.07.161.

[35] Liu H, Zhang Y, Li R, Sun X, Desilets S, Abou-Rachid H, Jaidann M, Lussier LS. Structural and morphological control of aligned nitrogen-doped carbon nanotubes. Carbon 2010;48:1498–507. https://doi.org/10.1016/j.carbon.2009.12.045.

[36] Lamour P, Fioux P, Ponche A, Nardin M, Vallat MF, Dugay P, Brum JP, Moreaud N, Pinvidic JM. Direct measurement of the nitrogen content by XPS in self-passivated TaNx thin films. Surf Int Anal 2008;40:11:1430–7. https://doi.org/10.1002/sia.2919.

[37] Ferrari AC, Robertson J. Interpretation of Raman spectra of disordered and amorphous carbon. Physical Review B 2000;61:20:14095–107. https://doi.org/10.1103/PhysRevB.61.14095.

[38] Tokoroyama T, Goto M, Umehara N, Nakamura T, Honda F. Effect of Nitrogen atoms desorption on the friction of the CNx coating against Si_3N_4 ball in Nitrogen gas. Tribology Letters 2004;22,215–20. https://doi.org/10.1007/s11249–006–9084–x.

[39] Cumpson PJ. Angle-resolved XPS and AES: depth-resolution limits and a general comparison of properties of depth-profile reconstruction methods. J Elect Spec Relat Phenomena 1995;73:1:25–52. https://doi.org/10.1016/0368–2048(94)02270–4.

[40] Tsuge M, Hama T, Kimura Y, Kouchi A, Watanabe N. Interactions of atomic and molecular hydrogen with a diamond-like carbon surface: H_2 formation and desorption. Astrophys J 2019;878:23:10pp. https://doi.org/10.3847/1538–4357/able4e.

[41] Yokota K, Tagawa M, Kitamura A, Matsumoto K, Yoshigoe A, Teraoka Y. Hydrogen desorption from a diamond-like carbon film by hyperthermal atomic oxygen exposure. Appl Surf Sci 2009;255:13-14:6710–4. https://doi.org/10.1016/j.apsusc.2009.02.064.

[42] Rusanov A, Fontaine J, Martin JM, Le Mogne T, Nevshupa R. Gas desorption during friction of amorphous carbon films. J Phys 2008;100:082050. https://doi.org/10.1088/1742–6596/100/8/082050.

[43] Nakayama K. Triboemission of electrons, ions, and photons from diamondlike carbon films and generation of tribomicroplasma. Surf Coat Technol 2004;188–189:599–604. https://doi.org/10.1016/j.surfcoat.2004.07.103.

[44] Miyahira Y, Tokoroyama T et al., In-situ observation for tribomicroplasma and transfer layer forming of carbon nitride coating. Tribologists 2011;56:6:378–384.

[45] Tokoroyama T, Kamiya M, Umehara N, Wang C, Diao DF. Influence of UV irradiation for low friction performance of CNx coatings. Lubrication Science 2012;24,129–39. https://doi.org/10.1002/ls.1168.

[46] Xu J, Hu W, Xie ZH, Munroe P. Reactive-sputter-deposited β-Ta_2O_5 and TaON nanoceramic coatings on Ti-6Al-4V alloy against wear and corrosion damage. Surf Coat Technol 2016;296:171–84. https://doi.org/10.1016/j.surfcoat.2016.04.004.

[47] Atanassova E, Dimitrova T, Koprinarova J. AES and XPS study of thin RF-sputtered Ta_2O_5 layers. Applied Surface Science 1995;84:193–202. https://doi.org/10.1016/0169–4332(94)00538–9.

[48] Deng X, Kousaka H, Tokoroyama T, Umehara N. Tribological behaviors of tetrahedral amorphous carbon (ta-C) coatings at elevated temperature. Tribol Int 2014;75:98–103. https://doi.org/10.1016/j.triboint.2014.04.002.

[49] Deng X, Kousaka H, Tokoroyama T, Umehara N. Thermal Stabiligy and High-Temperature Tribological Properties of a-C:H and Si-DLC Deposited by Microwave Sheath Voltage Combination Plasma. Tribology Online 2013;8:257–264. https://doi.org/10.2474/trol.8.257.

[50] Shi P, Sun J, Yan W, Zhou N, Zhang J, Zhang, J, Chen L, Qian L. Roles of phase transition and surface property evolution in nanotribological behaviors of H-DLC: Effects of thermal and UV irradiation treatments. Appl Surf Sci 2020;514:145960. https://doi.org/10.1016/j.spsusc.2020.145960.

[51] Kim JY, Magyari-Kope B, Nishi Y, Ahn JH. First-principles study of carbon impurity effects in the pseudo-hexagonal Ta_2O_5. Curr Appl Phys 2016;16:638–43. https://doi.org/10.1016/j.cap.2016.03.014.

[52] Du S, Zhang K, Wen M, Qin Y, Li R, Jin H, Bao X, Ren P, Zheng W. Optimizing the tribological behavior of tantalum carbide coating for the bearing in total hip joint replacement. Vacuum 2018;150:222–31. https://doi.org/10.1016/j.vacuum.2018.01.050.

[53] Martinez E, Wiklund U, Esteve J, Montala F, Carreras LL. Tribological performance on TiN supported molybdenum and tantalum carbide coatings in abrasion and sliding contact. Wear 2002;253:1182–7. https://doi.org/10.1016/S0043–1648(02)00245–4.

List of Figure Captions

Figure 1

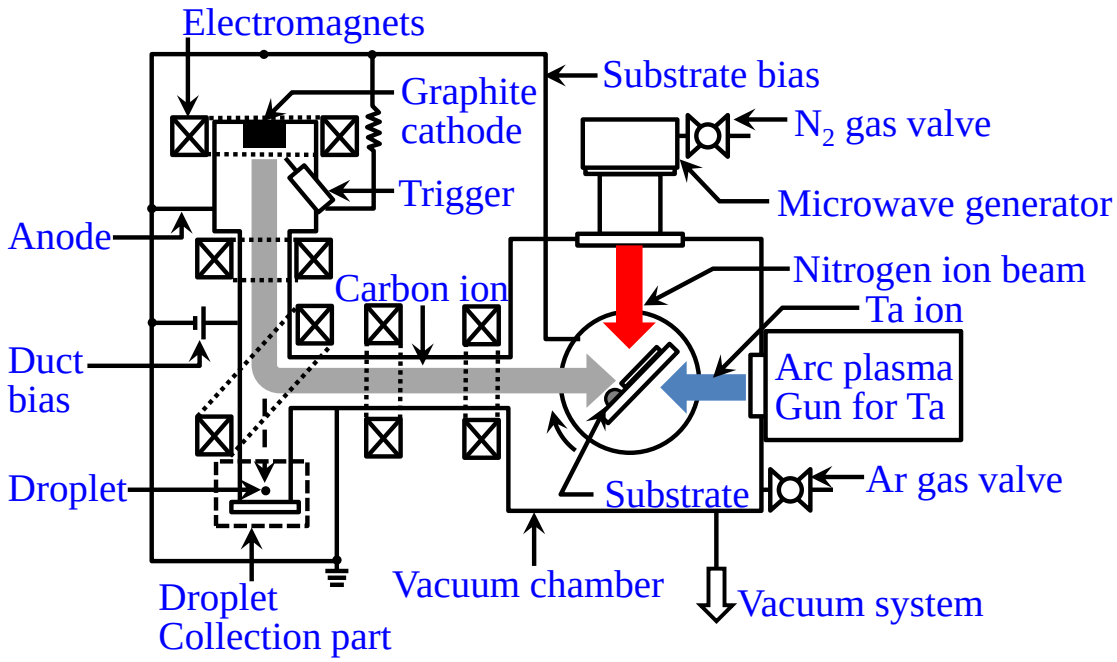
Electromagnets
Graphite cathode
Substrate bias
N_2 gas valve
Trigger
Microwave generator
Anode
Carbon ion
Nitrogen ion beam
Ta ion
Duct bias
Arc plasma Gun for Ta
Droplet
Substrate
Ar gas valve
Droplet Collection part
Vacuum chamber
Vacuum system

Figure 2

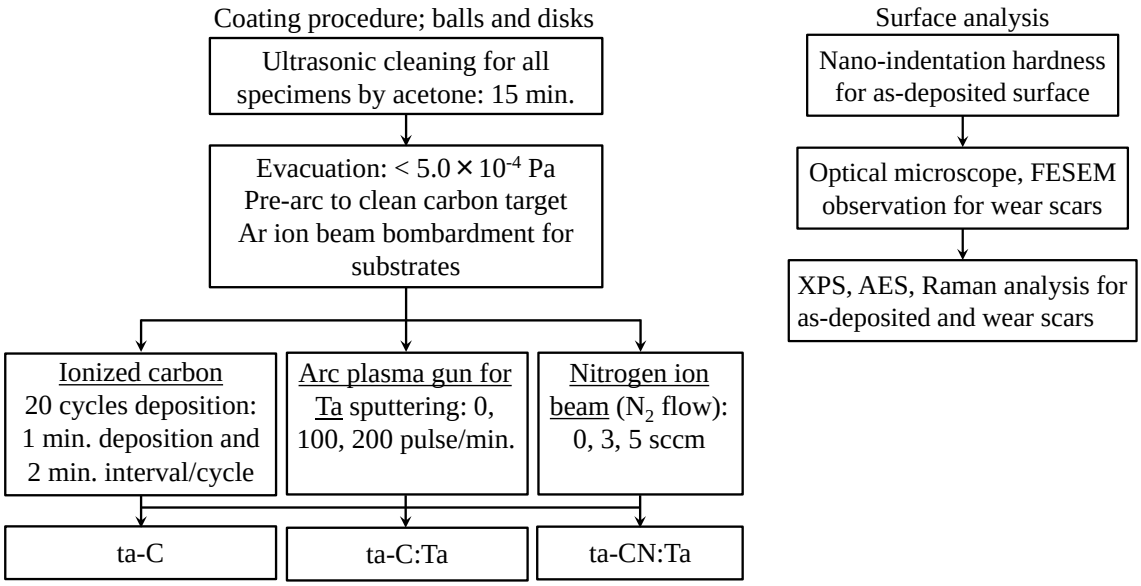
Coating procedure; balls and disks
Ultrasonic cleaning for all specimens by acetone: 15 min.
Evacuation: < 5.0 × 10-4 Pa
Pre-arc to clean carbon target
Ar ion beam bombardment for substrates
Ionized carbon
20 cycles deposition: 1 min. deposition and 2 min. interval/cycle
Arc plasma gun for Ta sputtering: 0, 100, 200 pulse/min.
Nitrogen ion beam (N2 flow): 0, 3, 5 sccm
ta-C
ta-C:Ta
ta-CN:Ta
Surface analysis
Nano-indentation hardness for as-deposited surface
Optical microscope, FESEM observation for wear scars
XPS, AES, Raman analysis for as-deposited and wear scars

Figure 3

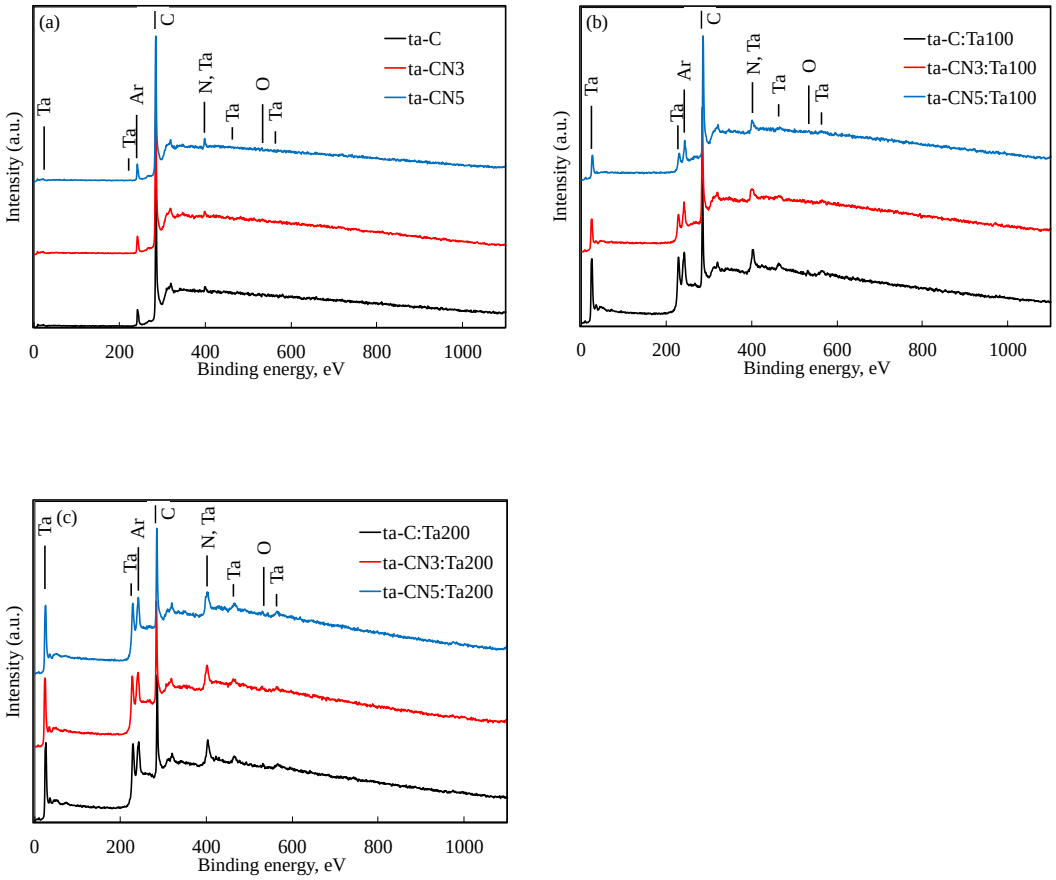
(a)
Ta
Ta
Ar
C
N, Ta
Ta
O
Ta
ta-C
ta-CN3
ta-CN5
Intensity (a.u.)
0
200
400
600
800
1000
Binding energy, eV
(b)
Ta
Ta
Ar
C
N, Ta
Ta
O
Ta
ta-C:Ta100
ta-CN3:Ta100
ta-CN5:Ta100
Intensity (a.u.)
0
200
400
600
800
1000
Binding energy, eV
(c)
Ta
Ta
Ar
C
N, Ta
Ta
O
Ta
ta-C:Ta200
ta-CN3:Ta200
ta-CN5:Ta200
Intensity (a.u.)
0
200
400
600
800
1000
Binding energy, eV

Figure 4

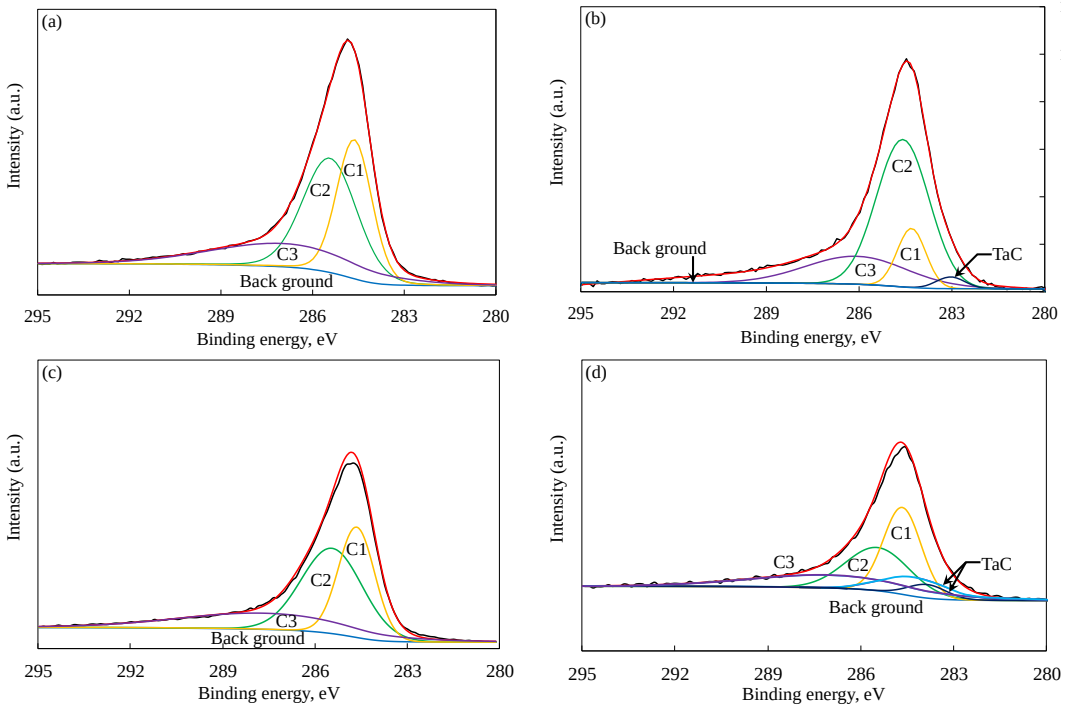
(a)
Intensity (a.u.)
C2
C1
C3
Back ground
295
292
289
286
283
280
Binding energy, eV
(b)
Intensity (a.u.)
C2
Back ground
C1
C3
TaC
295
292
289
286
283
280
Binding energy, eV
(c)
Intensity (a.u.)
C1
C2
C3
Back ground
295
292
289
286
283
280
Binding energy, eV
(d)
Intensity (a.u.)
C1
C3
C2
TaC
Back ground
295
292
289
286
283
280
Binding energy, eV

Figure 5

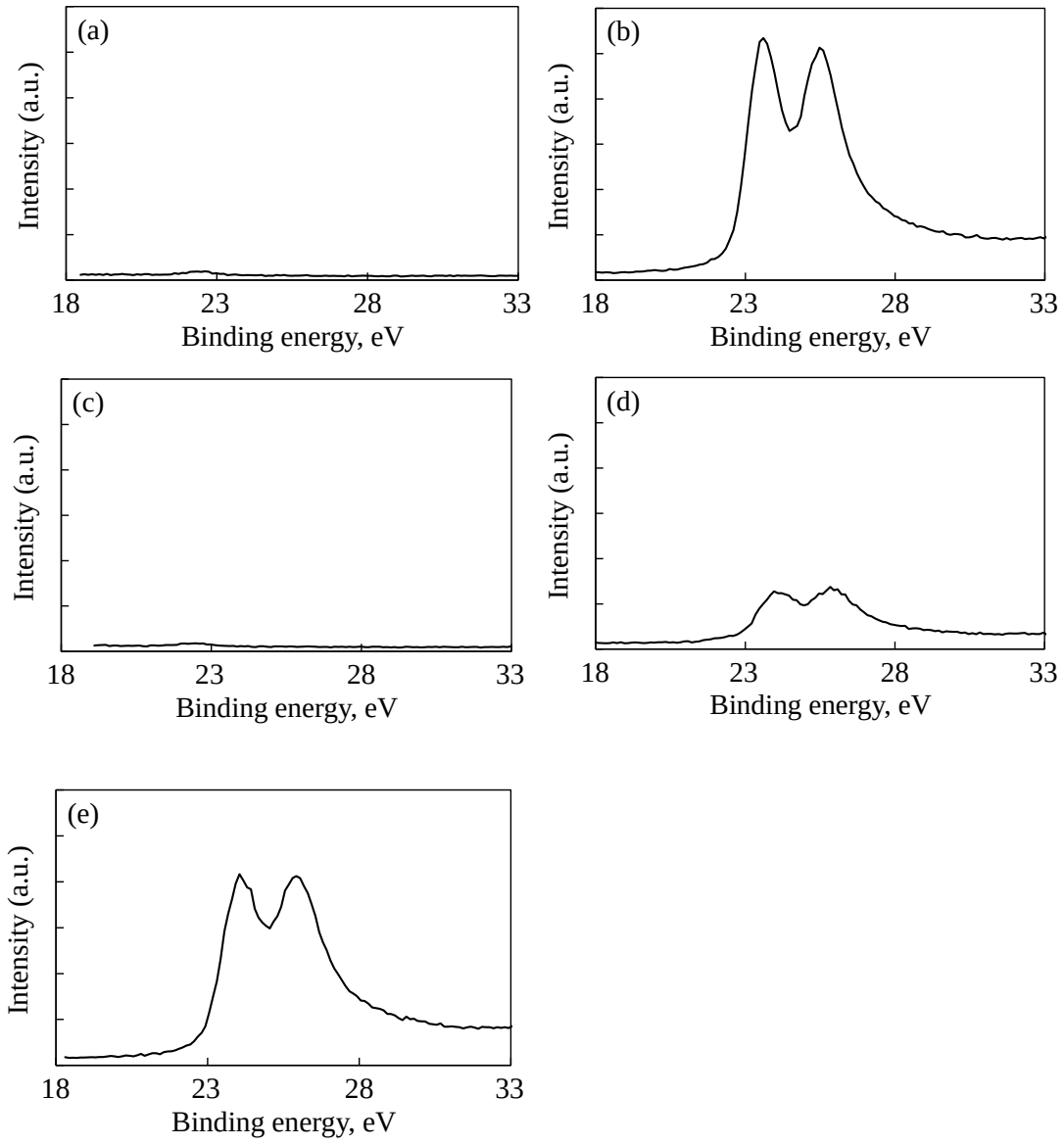
(a)
Intensity (a.u.)
18
23
28
33
Binding energy, eV
(b)
Intensity (a.u.)
18
23
28
33
Binding energy, eV
(c)
Intensity (a.u.)
18
23
28
33
Binding energy, eV
(d)
Intensity (a.u.)
18
23
28
33
Binding energy, eV
(e)
Intensity (a.u.)
18
23
28
33
Binding energy, eV

Figure 6

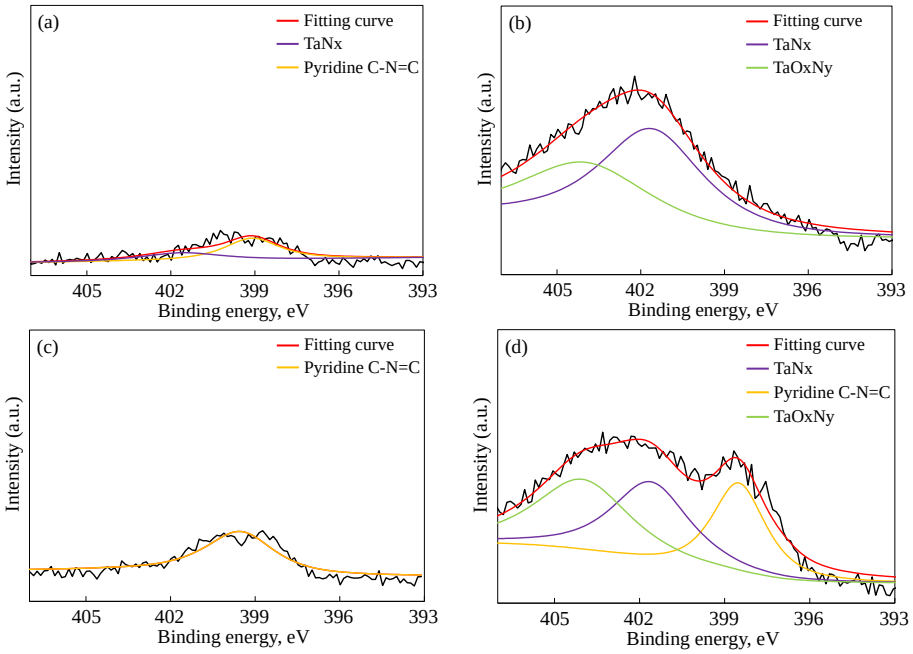
(a)
Fitting curve
TaNx
Pyridine C-N=C
Intensity (a.u.)
405
402
399
396
393
Binding energy, eV
(b)
Fitting curve
TaNx
TaOxNy
Intensity (a.u.)
405
402
399
396
393
Binding energy, eV
(c)
Fitting curve
Pyridine C-N=C
Intensity (a.u.)
405
402
399
396
393
Binding energy, eV
(d)
Fitting curve
TaNx
Pyridine C-N=C
TaOxNy
Intensity (a.u.)
405
402
399
396
393
Binding energy, eV

Figure 7

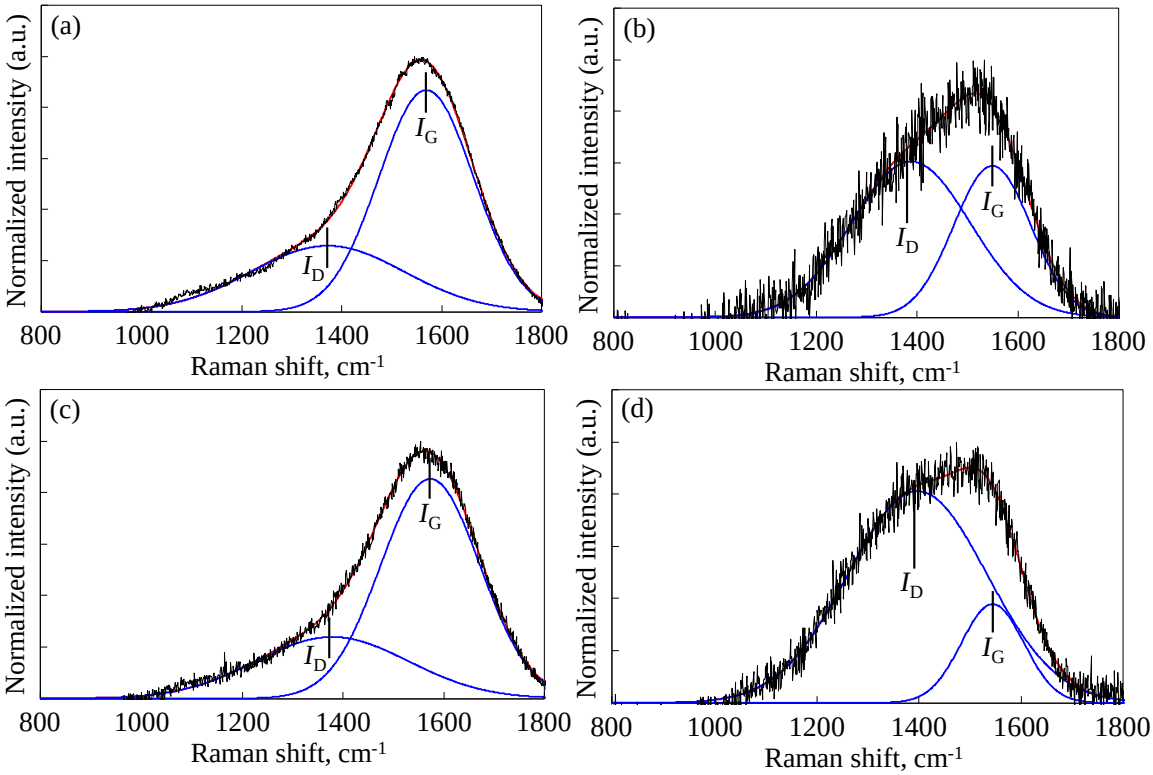
(a)
(b)
(c)
(d)
Normalized intensity (a.u.)
Raman shift, cm-1
800
1000
1200
1400
1600
1800
I_D
I_G

Figure 8

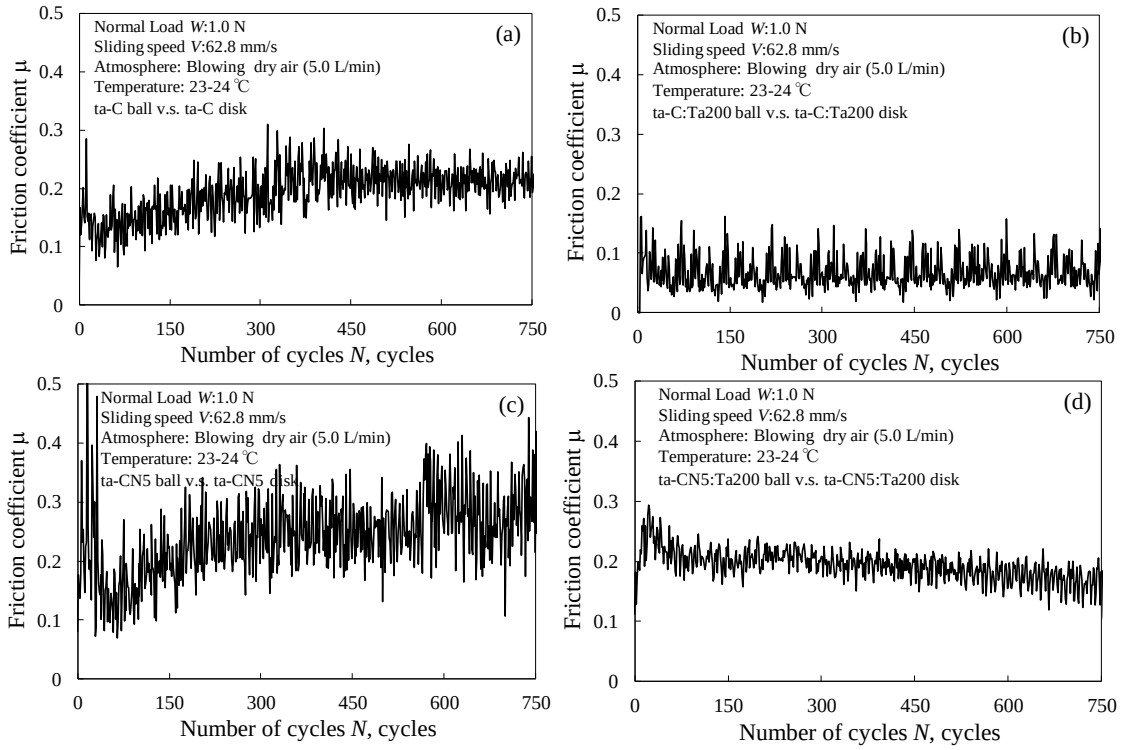
Normal Load W:1.0 N
Sliding speed V:62.8 mm/s
Atmosphere: Blowing dry air (5.0 L/min)
Temperature: 23-24 ℃
ta-C ball v.s. ta-C disk
(a)
Normal Load W:1.0 N
Sliding speed V:62.8 mm/s
Atmosphere: Blowing dry air (5.0 L/min)
Temperature: 23-24 ℃
ta-C:Ta200 ball v.s. ta-C:Ta200 disk
(b)
Normal Load W:1.0 N
Sliding speed V:62.8 mm/s
Atmosphere: Blowing dry air (5.0 L/min)
Temperature: 23-24 ℃
ta-CN5 ball v.s. ta-CN5 disk
(c)
Normal Load W:1.0 N
Sliding speed V:62.8 mm/s
Atmosphere: Blowing dry air (5.0 L/min)
Temperature: 23-24 ℃
ta-CN5:Ta200 ball v.s. ta-CN5:Ta200 disk
(d)
Friction coefficient μ
Number of cycles N, cycles
0
0.1
0.2
0.3
0.4
0.5
150
300
450
600
750

Figure 9

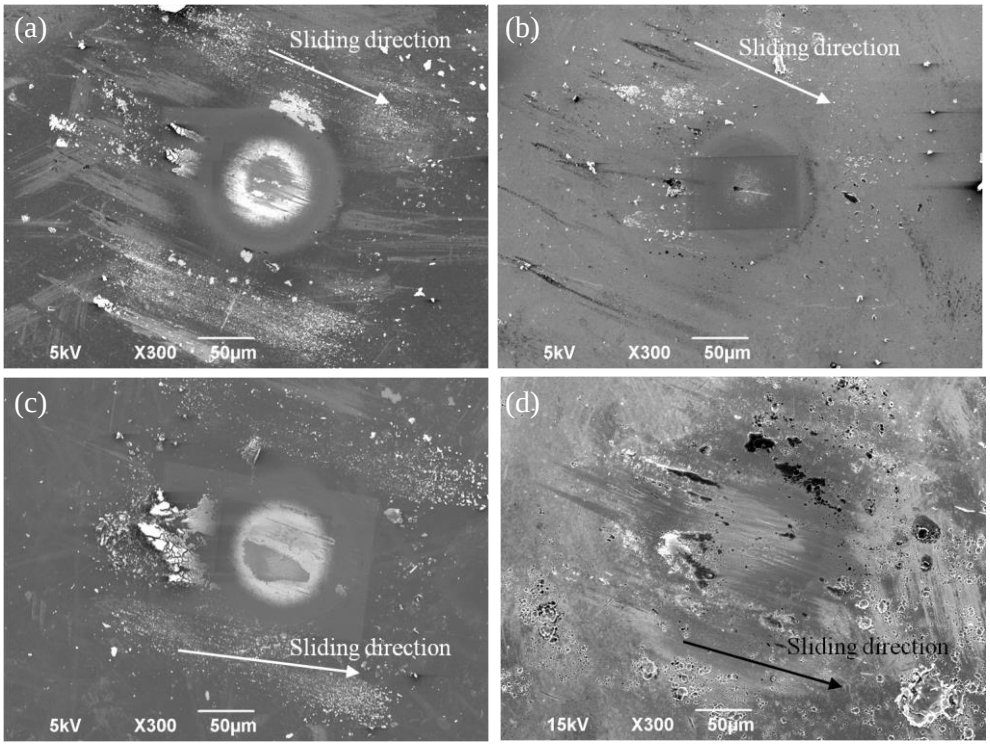
(a)
Sliding direction
5kV X300 50μm
(b)
Sliding direction
5kV X300 50μm
(c)
Sliding direction
5kV X300 50μm
(d)
Sliding direction
15kV X300 50μm

Figure 10

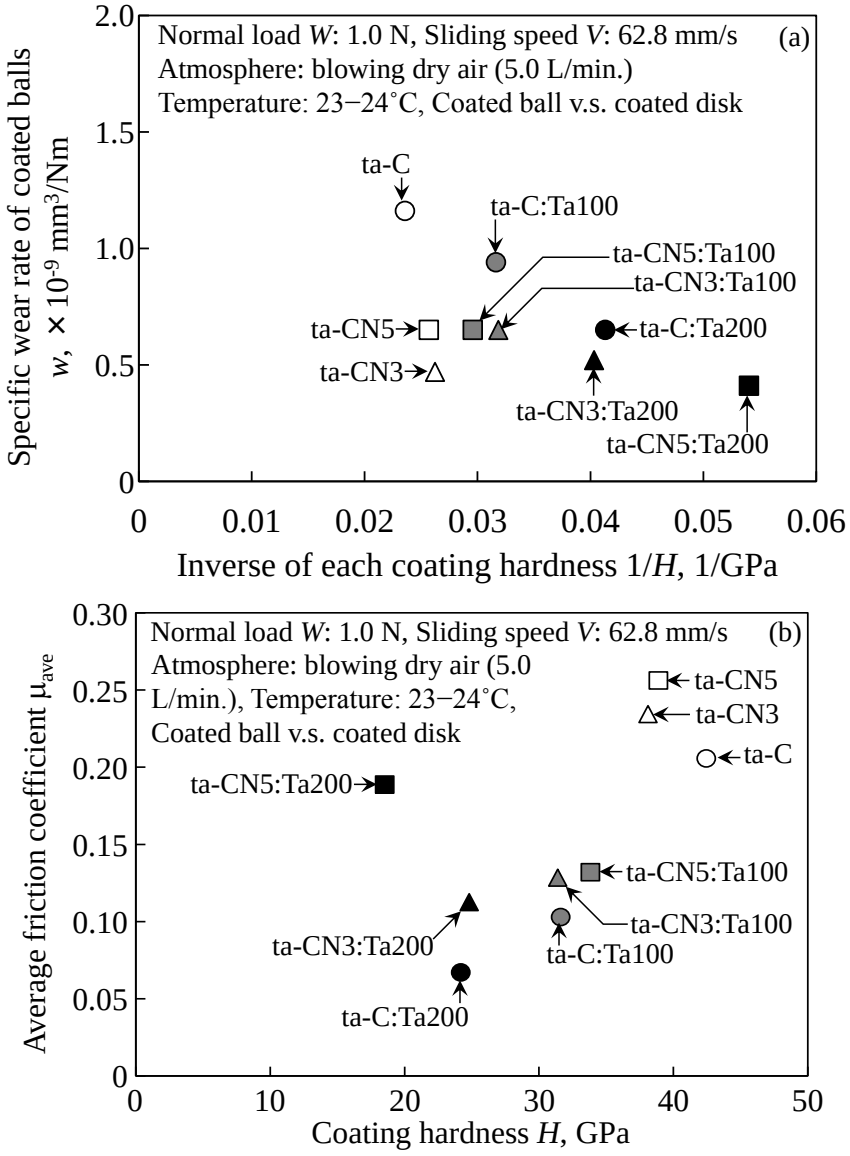
Normal load W: 1.0 N, Sliding speed V: 62.8 mm/s
Atmosphere: blowing dry air (5.0 L/min.)
Temperature: 23−24˚C, Coated ball v.s. coated disk
(a)
Specific wear rate of coated balls
w, × 10-9 mm3/Nm
ta-C
ta-C:Ta100
ta-CN5:Ta100
ta-CN3:Ta100
ta-CN5
ta-C:Ta200
ta-CN3
ta-CN3:Ta200
ta-CN5:Ta200
Inverse of each coating hardness 1/H, 1/GPa
Normal load W: 1.0 N, Sliding speed V: 62.8 mm/s
Atmosphere: blowing dry air (5.0 L/min.), Temperature: 23−24˚C,
Coated ball v.s. coated disk
(b)
ta-CN5
ta-CN3
ta-C
ta-CN5:Ta200
ta-CN5:Ta100
ta-CN3:Ta100
ta-CN3:Ta200
ta-C:Ta100
ta-C:Ta200
Average friction coefficient μave
Coating hardness H, GPa

Figure 11

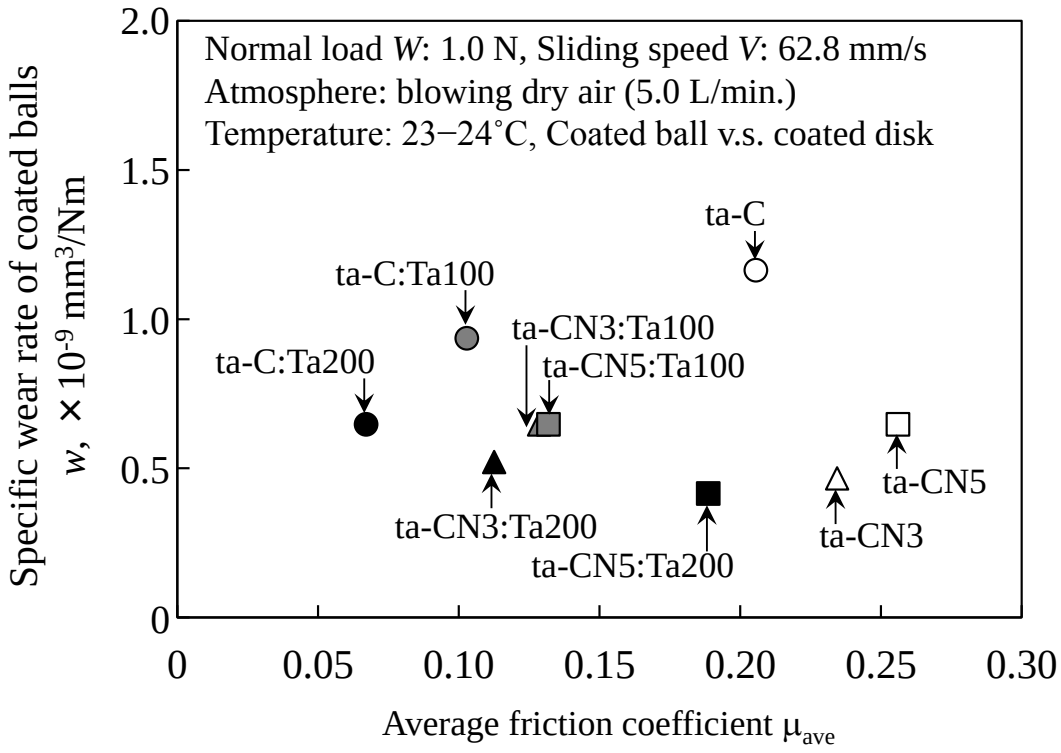
Normal load W: 1.0 N, Sliding speed V: 62.8 mm/s
Atmosphere: blowing dry air (5.0 L/min.)
Temperature: 23−24˚C, Coated ball v.s. coated disk
Specific wear rate of coated balls
w, × 10-9 mm3/Nm
Average friction coefficient μave
ta-C
ta-C:Ta100
ta-CN3:Ta100
ta-CN5:Ta100
ta-C:Ta200
ta-CN5
ta-CN3:Ta200
ta-CN3
ta-CN5:Ta200
0
0.5
1.0
1.5
2.0
0.05
0.10
0.15
0.20
0.25
0.30

Figure 12

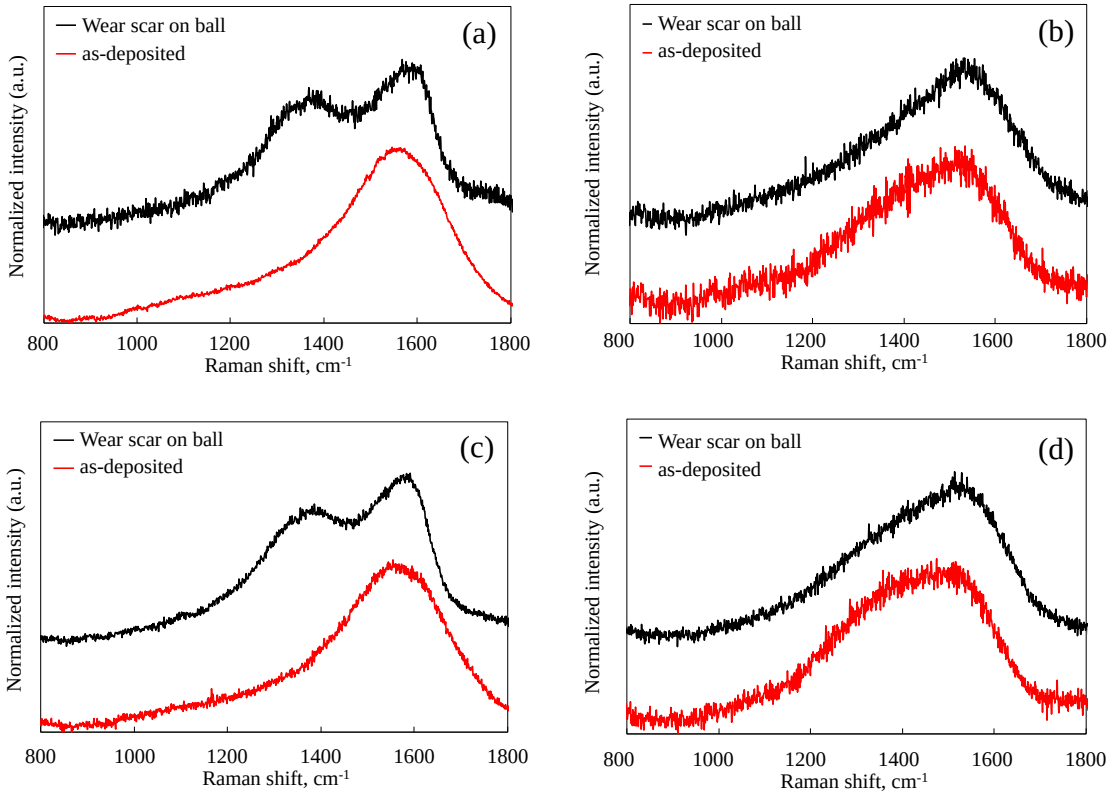
Wear scar on ball
as-deposited
(a)
Normalized intensity (a.u.)
800
1000
1200
1400
1600
1800
Raman shift, cm-1
Wear scar on ball
as-deposited
(b)
Normalized intensity (a.u.)
800
1000
1200
1400
1600
1800
Raman shift, cm-1
Wear scar on ball
as-deposited
(c)
Normalized intensity (a.u.)
800
1000
1200
1400
1600
1800
Raman shift, cm-1
Wear scar on ball
as-deposited
(d)
Normalized intensity (a.u.)
800
1000
1200
1400
1600
1800
Raman shift, cm-1

Figure 13

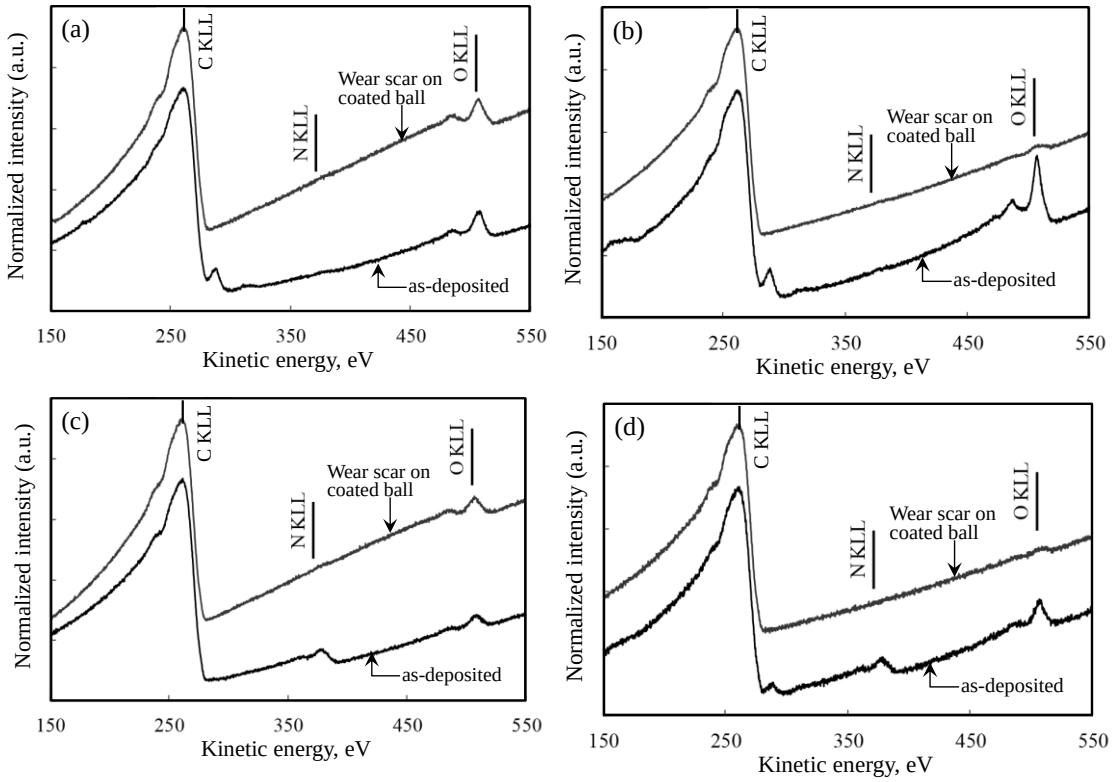
(a)
C KLL
N KLL
O KLL
Wear scar on coated ball
as-deposited
Normalized intensity (a.u.)
150
250
350
450
550
Kinetic energy, eV
(b)
C KLL
N KLL
O KLL
Wear scar on coated ball
as-deposited
Normalized intensity (a.u.)
150
250
350
450
550
Kinetic energy, eV
(c)
C KLL
N KLL
O KLL
Wear scar on coated ball
as-deposited
Normalized intensity (a.u.)
150
250
350
450
550
Kinetic energy, eV
(d)
C KLL
N KLL
O KLL
Wear scar on coated ball
as-deposited
Normalized intensity (a.u.)
150
250
350
450
550
Kinetic energy, eV

Figure 14

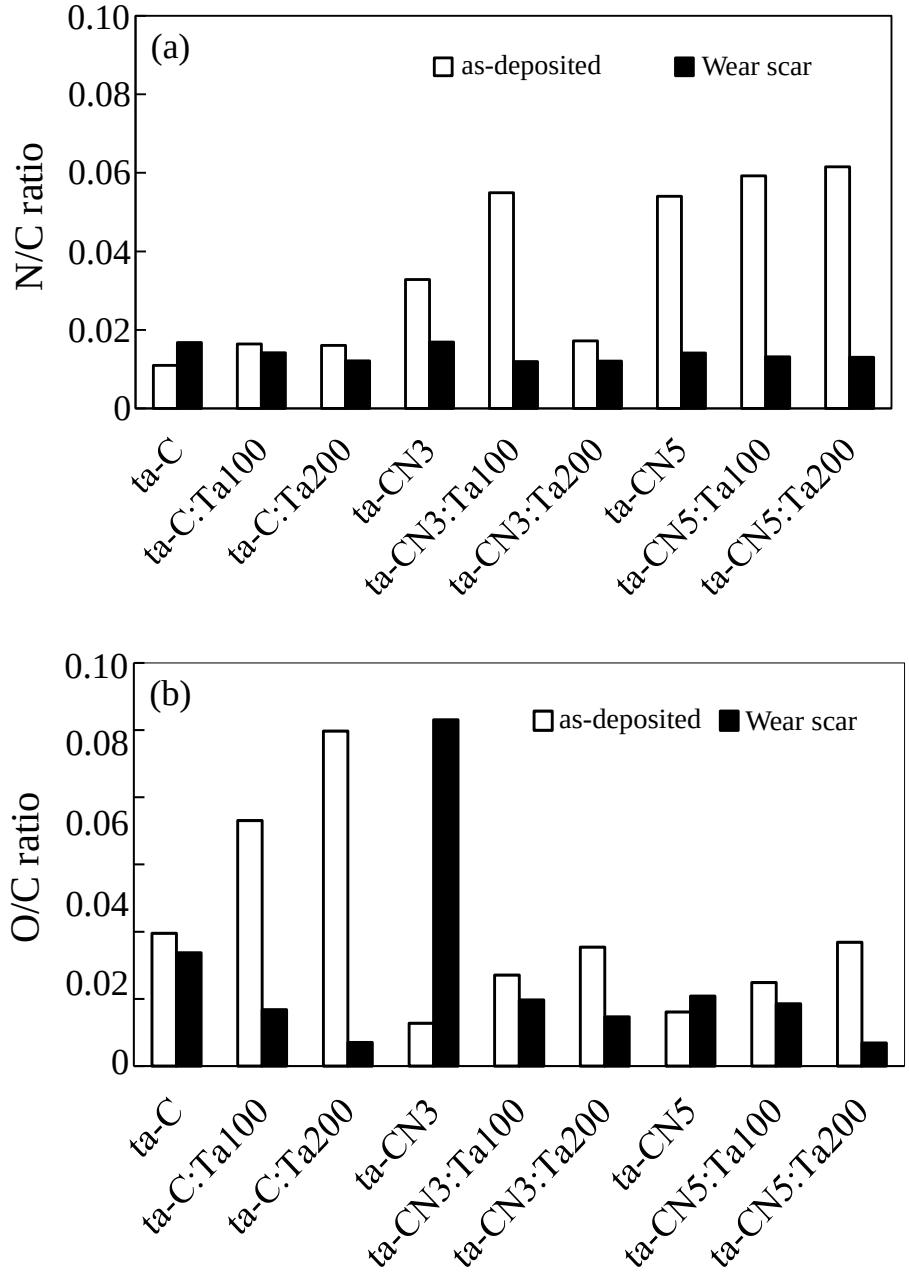
(a)
as-deposited
Wear scar
N/C ratio
0.10
0.08
0.06
0.04
0.02
0
ta-C
ta-C:Ta100
ta-C:Ta200
ta-CN3
ta-CN3:Ta100
ta-CN3:Ta200
ta-CN5
ta-CN5:Ta100
ta-CN5:Ta200
(b)
as-deposited
Wear scar
O/C ratio
0.10
0.08
0.06
0.04
0.02
0
ta-C
ta-C:Ta100
ta-C:Ta200
ta-CN3
ta-CN3:Ta100
ta-CN3:Ta200
ta-CN5
ta-CN5:Ta100
ta-CN5:Ta200

Figure 15

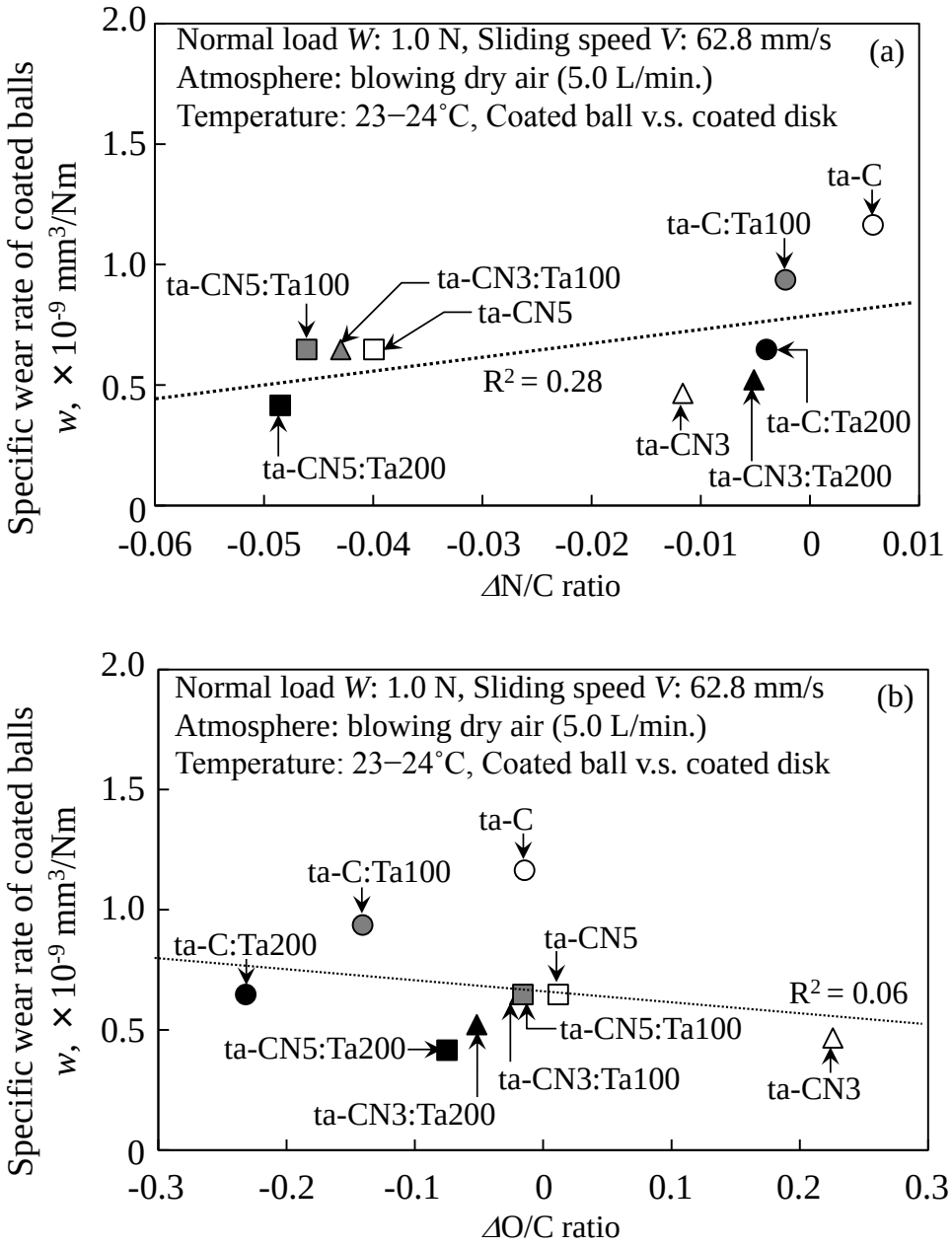
Normal load W: 1.0 N, Sliding speed V: 62.8 mm/s
Atmosphere: blowing dry air (5.0 L/min.)
Temperature: 23−24˚C, Coated ball v.s. coated disk
(a)
Specific wear rate of coated balls
w, × 10-9 mm3/Nm
ta-C
ta-C:Ta100
ta-CN5:Ta100
ta-CN3:Ta100
ta-CN5
R2 = 0.28
ta-C:Ta200
ta-CN3
ta-CN3:Ta200
ta-CN5:Ta200
ΔN/C ratio
(b)
ta-C
ta-C:Ta100
ta-C:Ta200
ta-CN5
R2 = 0.06
ta-CN5:Ta100
ta-CN5:Ta200
ta-CN3:Ta100
ta-CN3
ta-CN3:Ta200
ΔO/C ratio

Figure 16

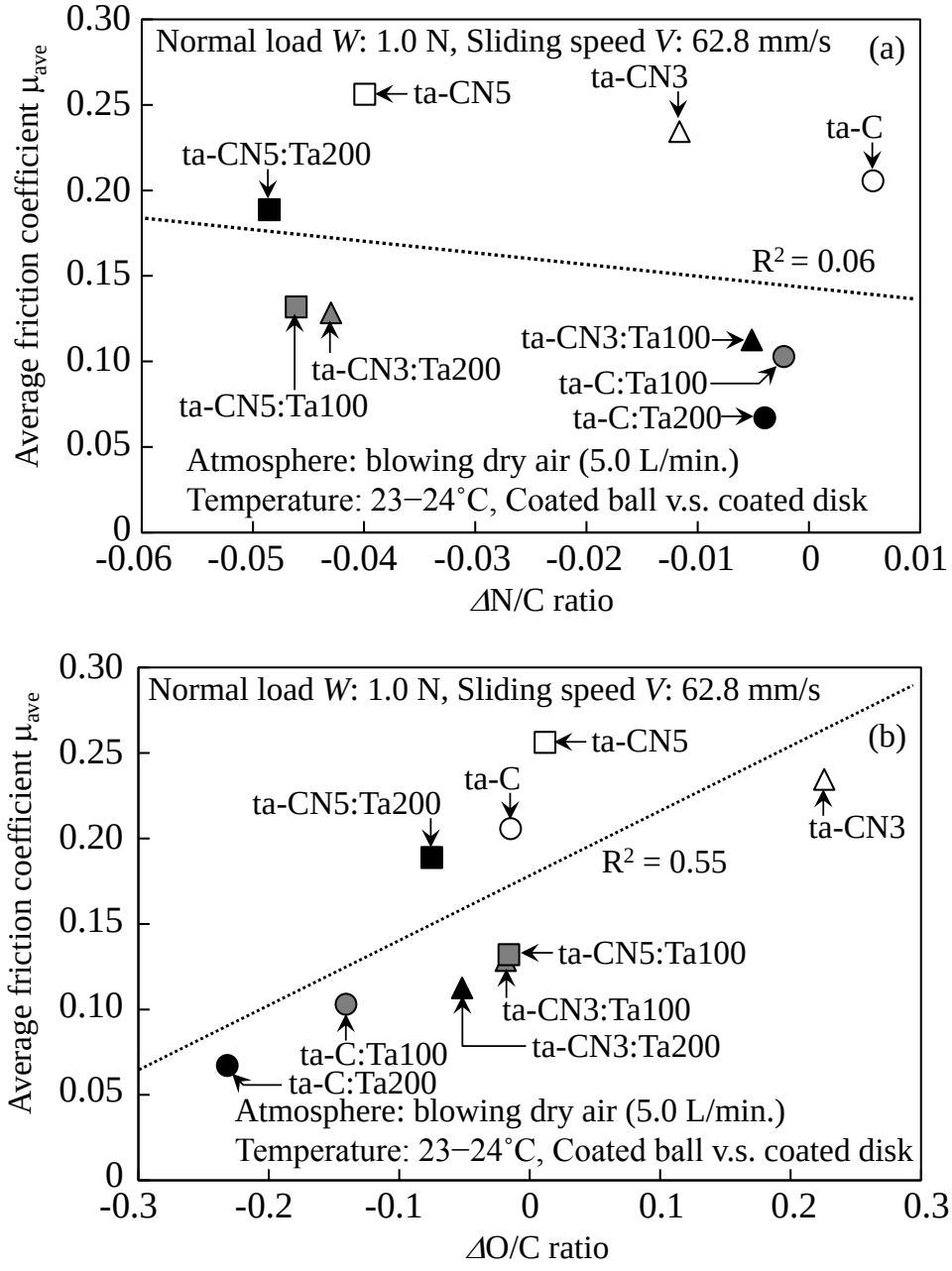
Normal load W: 1.0 N, Sliding speed V: 62.8 mm/s
(a)
ta-CN5
ta-CN3
ta-C
ta-CN5:Ta200
R2 = 0.06
ta-CN3:Ta100
ta-CN3:Ta200
ta-C:Ta100
ta-CN5:Ta100
ta-C:Ta200
Atmosphere: blowing dry air (5.0 L/min.)
Temperature: 23−24˚C, Coated ball v.s. coated disk
Average friction coefficient μave
ΔN/C ratio
0.30
0.25
0.20
0.15
0.10
0.05
0
-0.06
-0.05
-0.04
-0.03
-0.02
-0.01
0
0.01
Normal load W: 1.0 N, Sliding speed V: 62.8 mm/s
(b)
ta-CN5
ta-C
ta-CN5:Ta200
ta-CN3
R2 = 0.55
ta-CN5:Ta100
ta-CN3:Ta100
ta-C:Ta100
ta-CN3:Ta200
ta-C:Ta200
Atmosphere: blowing dry air (5.0 L/min.)
Temperature: 23−24˚C, Coated ball v.s. coated disk
Average friction coefficient μave
ΔO/C ratio
0.30
0.25
0.20
0.15
0.10
0.05
0
-0.3
-0.2
-0.1
0
0.1
0.2
0.3

Table 1

Deposition time *t*, min	20
Ratio of interval, deposition[s]/interval[s]	60/120
Arc current A_c, A	50
Substrate bias voltage V_s, -V	100
Duct bias voltage V_d, V	15
Rotation speed of substrate, rpm	5
Nitrogen mass flow, sccm	0, 3, 5
Anode current I_A, mA	50
Screen bias voltage V_{sc}, V	1500
Acceleration bias voltage V_{acc}, V	-100
Voltage between anode and cathode $V_{a\text{-}c}$, V	200
Number of discharge D_n, pulse/min	0, 100, 200

Table 2

	C (at.%)	N (at.%)	O (at.%)	Ta (at.%)
ta-C	97.76	1.46	0.78	0.00
ta-C:Ta100	88.54	2.20	1.43	7.83
ta-C:Ta200	88.61	0.49	1.14	9.76
ta-CN3	97.57	1.65	0.79	0.00
ta-CN3:Ta100	93.13	4.09	0.38	2.40
ta-CN3:Ta200	88.35	4.90	1.33	5.42
ta-CN5	96.49	3.32	0.19	0.00
ta-CN5:Ta100	94.16	4.30	0.00	1.53
ta-CN5:Ta200	86.54	7.46	0.74	5.27

Table 3

	ta-C	ta-CN3	ta-CN5	ta-C:Ta100	ta-CN3:Ta100	ta-CN5:Ta100	ta-C:Ta200	ta-CN3:Ta200	ta-CN5:Ta200
Hardness *H*, GPa	42.4	38.1	38.9	31.6	31.4	33.8	24.2	24.8	18.5
Young's modulus E, GPa	415.6	365.0	289.4	361.1	332.9	242.6	344.7	282.0	207.7